ARTICLE

JOURNAL OF
Applied Polymer WILEY
SCIENCE

Sustainable textile fibers of bioderived polylactide/poly(pentamethylene 2,5-furanoate) blends

Davide Perin[1] (ORCID) | **Giulia Fredi**[1] | **Daniele Rigotti**[1] | **Michelina Soccio**[2] |
Nadia Lotti[2] | **Andrea Dorigato**[1]

[1]Department of Industrial Engineering and INSTM Research Unit, University of Trento, Trento, Italy

[2]Department of Civil, Chemical, Environmental, and Materials Engineering, University of Bologna, Bologna, Italy

Correspondence
Davide Perin and Andrea Dorigato, Department of Industrial Engineering and INSTM Research Unit, University of Trento, Via Sommarive 9 38123, Trento, Italy.
Email: davide.perin-1@unitn.it, andrea.dorigato@unitn.it

Funding information
Fondazione Cassa Di Risparmio Di Trento E Rovereto, Grant/Award Number: 2020.0265; Cost Action Fur4sustain, Grant/Award Number: CA18220

Abstract

Furanoate polyesters are emerging as promising bioderived polymers that could replace petrochemical-derived polyesters in several applications, for example, the textile field. Here, sustainable and fully bioderived fibers are wet-spun by blending poly(lactic acid) (PLA) and poly(pentamethylene 2,5-furanoate) (PPeF), with up to 50 wt% of PPeF. PLA/PPeF blends result as immiscible, with PPeF domains homogeneously distributed within the PLA matrix, as shown by scanning electron micrographs. The immiscibility is confirmed by differential scanning calorimetry, as the glass transition temperature of PLA is unaffected by PPeF. The immiscibility and poor adhesion between PLA and PPeF are responsible for the decrease in stress at break and elongation at break from 30.1 MPa and 127%, of PLA fibers, to 3.5 MPa and 1.9%, at high PPeF amounts. However, the addition of PPeF strongly decreases the PLA's tendency to absorb water and retain the processing solvents, showing a mass loss decrease from 3.1% for PLA fibers to 1% for fibers containing 50 wt% PPeF, thereby addressing one of the main drawbacks of PLA. These results, although preliminary, offer new directions for future works on innovative and sustainable fibers based on furanoate polyesters.

KEYWORDS
biopolymers and renewable polymers, blends, fibers, mechanical properties, textiles

1 | INTRODUCTION

Plastics are one of the most widely used materials and it is sometimes referred to as one of the greatest innovations of the millennium. Plastic products achieved such an extensive market thanks to their low density, limited price, versatility, and recyclability.[1] Therefore, the global annual plastics production has increased by approximately 10% each year since 1950.[2] In 2018, the worldwide production of plastics amounted to 360 million tons, with a forecast of 500 million tons in 2025.[3,4] As a drawback, about 381 million tons of plastic wastes are generated every year. Due to the non-optimal management of plastic waste, global pollution deriving from these products has strongly increased.[5] Thus, in order to favor the switch from a linear to a circular economy,[6] industries and governments have recently changed their policy, moving towards sustainable use of plastic materials and also the use of sustainable processes.[7] For this reason, the last decades have seen an increasing interest in the so-called

bioplastics,[8–12] that are polymers that are biodegradable and/or produced starting from renewable resources.[13] The most widely used bioplastics are poly(lactic acid) (PLA),[14] polyhydroxyalkanoates (PHAs),[15] poly(ε-caprolactone) (PCL),[16] thermoplastic starch (TPS),[17] and poly(vinyl alcohol) (PVA).[18]

PLA is a biopolymer exhibiting a tensile modulus of approximately 3 GPa, good mechanical strength, improved workability, and higher transparency in comparison to other bio-based biopolymers. Furthermore, it is also compostable and recyclable.[14] For all these reasons, PLA represents an attractive alternative to traditional plastics for packaging and textile applications .[19–21] On the other hand, PLA is characterized by a low deflection temperature and, if used as a container for hot food or beverages, it could be subjected to a partial loss of dimensional stability. Furthermore, PLA generally presents rather limited fracture toughness with respect to oil-based polymers.[22] These drawbacks could be partially or totally overcome through the blending technology.

Even though the majority of polymer blends are immiscible, blending process could improve and/or tailor the physical properties of the resulting plastics in a more economical way with respect to the synthesis of new matrices.[23–26] A physical polymer blend is defined as a mechanical mixture, generally obtained after a short time mixing (no chemical reactions can appreciably occur in these conditions), in which at least two polymers are involved, to produce a new material possessing different properties in comparison to its constituents.[27,28] An interesting class of bio-based polymers that could be blended with PLA are polyesters of 2,5-furandicarboxylic acid (FDCA), obtained from the polycondensation reaction of this latter with different diols. A wide variety of homopolymers[29,30] or copolymers,[31–35] capable of replacing the traditional polyesters, can be thus synthesized. The most important and widely studied polyesters obtained from FDCA are poly(ethylene 2,5 furandicarboxylate) (PEF), which is the bioderived counterpart of polyethylene terephthalate (PET).[36] It possesses good mechanical and thermal properties and also improved barrier properties with respect to PET.[37] On the other hand, it is characterized by a brittle behavior at room temperature, and this feature (together with the elevated price of FDCA) limited its use in different industrial applications. Besides PEF several homopolyesters, derived from the polymerization reaction between FDCA and aliphatic diols with a higher number of carbon atoms, have been recently synthesized, like poly(propylene 2,5-furandicarboxylate) (PPF),[38] poly(butylene 2,5-furandicarboxylate) (PBF),[39,40] poly(pentamethylene 2,5-furanoate) (PPeF),[41–44] poly (hexamethylene 2,5-furandicarboxylate) (PHF),[42,45] poly(octylene 2,5-furandicarboxylate) (POF),[46] poly

(decylene 2,5-furandicarboxylate) (PDeF)[47,48] and poly(dodecylene 2,5-furandicarboxylate) (PDoF).[49] The direct consequence of the increase in the number of carbon atoms of the diol is the decrease of the thermo-mechanical properties of the resulting furan-based polyester furanoate, in terms of elastic modulus (E), glass transition temperature (T_g), and melting temperature (T_m).[42,50] However, the increment of the alkyl chain length results in a more ductile behavior, making these biopolymers suitable for packaging or textile applications.[51] Up to now, only a few works are present in the literature on the characterization of furan-based polymers such as PBF, PPeF, PHF, POF, and PDoF.[38,41,46,49] In addition, only few works dealing with the blending of PLA with furan-based polyesters can be found.

Poulopoulou et al.[52] investigated a series of blends based on PBF combined with several polyesters such as PLA, PET, poly(propylene terephthalate) (PPT), poly(butylene naphthalate) (PBN), and polycarbonate (PC). Differential scanning calorimetry (DSC) tests and polarized light microscopy on PBF/PLA blends showed that the two polymers were essentially immiscible. Long et al.[53] studied PLA/PBF blends, highlighting that these blends were immiscible but possessed high reflectivity, enabling thus the production of shining surface products This increase in reflectivity was correlated to two main reasons, namely the increase in surface area of PLA lamellar crystals and the relatively large difference in the refractive index of PLA (1.443) and PBF (1.553). Furthermore, it was also shown that through the addition of only 5 wt% of PBF to PLA, the elongation at break increased about 18 times in comparison to neat PLA, without decreasing the stiffness and the yield resistance.[54] Fredi et al.[55] have recently performed a comprehensive study concerning the blending of PLA with PBF, PHF, POF, and PDeF for sustainable packaging applications. They have shown that by adding 5 wt% of PDeF to PLA, both the elastic modulus and the stress at break (σ_b) were slightly decreased, but the essential work of fracture (w_e) increased by 103%, and the strain at break (ε_b) by +996% in comparison to neat PLA films. The observed enhancement of the fracture toughness can be potentially exploited in the production of novel bio-based packaging films.

An interesting candidate for the preparation of PLA based blends could be PPeF, synthesized for the first time using FDCA and 1,5-pentanediol in a melt polycondensation process by Tsanaktsis et al.[41] PPeF is an amorphous polymer possessing low elastic modulus and elevated elongation at break. It also presents outstanding barrier properties to O_2 and CO_2, comparable to those of ethylene vinyl alcohol (EVOH).[44] As reported by Papageorgiou et al.,[30] also semicrystalline PPeF could be synthesized, depending on the molecular weight and the processing conditions. Martinez-Tong et al.[43] performed a comprehensive study on the thermal properties of PPeF

undergoing different thermal histories. From the DSC analysis, they observed that PPeF was amorphous, but if the PPeF sample was kept for 18 months at room temperature, it reported multiple melting phenomena, which is typical of semicrystalline polymers.[43] In a parallel work of our group, thin films made of PLA/PPeF have been prepared through solvent casting and the thermomechanical properties of the obtained materials were strictly correlated to their microstructural features. The drop of stiffness and failure properties upon PPeF introduction was largely compensated by a strong enhancement of strain at break, especially with a furanoate amount of 30 wt%.

PLA fibers offer the opportunity to overcome the poor sustainability of traditional PET based textiles.[56–58] Furthermore, PLA fibers are characterized by superior UV properties and reduced smoke characteristics, in case of fire, in comparison to PET fibers. For these reasons, PLA fibers could be potentially applied in nonwoven fabrics, clothes, drapes, upholstery, and covers.[59–61] Thus, blending furan-based polymers with PLA could lead to novel eco-sustainable fibers with improved and/or tailored physical properties. Quite surprisingly, these blends have not yet been studied and to the best of our knowledge, no papers are reported in the literature. Therefore, our work is focused on the production, for the first time, of novel PLA/PPeF fibers through wet spinning process. A comprehensive microstructural and thermo-mechanical characterization has been carried out, in order to highlight the effect of the addition of different amounts of PPeF to PLA, and to assess the suitability of the resulting materials for textile applications.

2 | MATERIALS AND METHODS

2.1 | Materials

The PLA used in this work was Ingeo® biopolymer 4032D (density = 1.24 g/cm^3, MFI at 210°C and 2.16 kg = 7 g/10 min), produced by NatureWorks LLC (Minnetonka, USA) in pellets form. Poly(pentamethylene furanoate) (PPeF) was synthesized at lab-scale through a solvent-free polycondensation process, according to the procedure described in the work of Guidotti et al.[44] PPeF was characterized by a number average molecular weight (M_n) of 29,600 Da, a polydispersity index (Đ) equal to 2.4, and a T_g of about 13°C.[44] Regarding the solvents, chloroform (HPLC grade), ethanol (purity 99.9%), and methanol (purity 99.9%) were purchased by Carlo Erba Reagents Srl. PLA pellets were stored in a drying oven at a temperature of 50°C before processing while the other materials were used as received.

2.2 | Samples preparation

Fibers were obtained by means of a wet spinning process. Neat PLA and PLA/PPeF mixtures were dissolved at different relative amounts in chloroform, as this solvent was reported to be capable of dissolving both PLA and furan-based polyesters with a relatively long alkyl chain, such as PPeF.[42,62,63] For producing the solution to be spun, 0.75 g of polymer mixtures were dissolved in 5 ml of chloroform, and the resulting solutions were magnetically stirred at 40°C for 3 h, and subsequently mildly ultrasonicated for 10 min in a Labsonic LBS1 bath (Falc Instruments Srl, Bergamo). This last step was fundamental to remove the small air bubbles that could be trapped inside the mixture during the stirring process since they might lead to porosity or defects in the produced fibers. The spinning process was performed with a lab-made device illustrated in Figure 1. The glass syringe containing the polymer solution was fixed on a Harvard apparatus Model 11 Single Syringe 55-1199 (Harvard apparatus Inc.), connected with an 18 gauge needle, that was subsequently sealed into the non-solvent bath. The extrusion rate was set at 0.007 ml/min and the take-up rollers speed at 5 mm/s since these process parameters were found to be suitable for the production of a continuous fiber. The solution was then spun into a non-solvent bath, aiming to remove the chloroform and produce thus solvent-free continuous fibers. The non-solvent bath was a solution containing 80 vol% of ethanol and 20 vol% of methanol by the fact that both these solvents induced PLA crystallization, without dissolving PLA or PPeF, and reported good miscibility with chloroform.[64] The obtained fibers were left 24 h in air to allow complete solvent evaporation and then stored in a desiccator.

The wet spinning process led to the production of neat PLA fibers and PLA/PPeF fiber blends with PPeF concentration ranging from 10 to 50 wt%. Each sample was labeled as PLA_xPPeF, where x represents the weight content of PPeF in the polymer blend. Neat PPeF resulted to be non-spinnable, because it is an amorphous polymer characterized by elastomeric properties.[65,66] The specimen related to the as received PPeF was simply labeled as PPeF. Table 1 reports the list of the produced fibers, the nominal weight and volume fraction of PPeF, and the mean diameter of the produced fibers, which was determined through a light microscope, and at least 15 fibers were measured (see Section 2.3). It can be immediately seen that, regardless of the PPeF concentration, fibers with a mean size lower than 100 μm were produced, and their diameter did not seem to be substantially influenced by the PPeF amount.
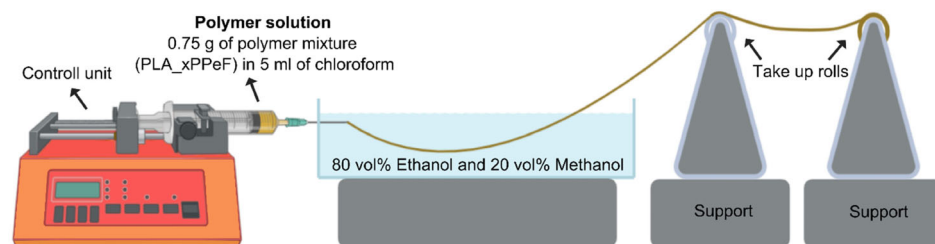
Sample	PAF content (wt%)	PAF content (vol%)	Mean diameter (μm)
PLA	0	0	83 ± 10
PLA_10PPeF	10	9.5	96 ± 9
PLA_20PPeF	20	19.1	79 ± 16
PLA_30PPeF	30	28.8	90 ± 12
PLA_50PPeF	50	48.6	85 ± 11

TABLE 1 List of prepared fiber blends

2.3 | Experimental techniques

2.3.1 | Microstructural and chemical properties

Light microscope (LM) micrographs of the spun fiber blends were acquired with a CH-9435 Heerbrugg optical microscope (Heerbrugg, Switzerland). By following the experimental procedure developed by Fredi et al.,[67] LM micrographs of the fiber cross-section were acquired by winding the obtained fibers to a poly(methyl methacrylate) (PMMA) parallelepiped, which was subsequently embedded in easy to handle epoxy beads. ImageJ® software (release 1.45) was then used to measure the diameter of the fibers. Both the lateral surface and the cryofractured surface of the fiber blends was investigated through field-emission scanning electron microscopy (FESEM) by using a Zeiss Supra 60 (Carl Zeiss AG) microscope, operating at an acceleration potential of 2.5 kV. Prior to the observations, the samples were sputtered with a platinum–palladium coating, to render them conductive. Fourier transformed infrared (FTIR) spectroscopy was performed in attenuated total reflectance (ATR) mode by using a Perkin-Elmer Spectrum One instrument (Perkin Elmer GmbH), equipped with a ZnSe crystal and operating in a wavenumber range 650–4000 cm^{-1}. Furthermore, in order to reduce the signal-to-noise-ratio, a hundred scans were collected for each spectrum (resolution 4 cm^{-1}).

2.3.2 | Thermal properties

DSC was performed with a Mettler DSC 30 calorimeter (Mettler Toledo, Inc.) at a heating rate of 10°C/min in a temperature range from −50 to 250°C, under a nitrogen flow of 100 ml/min. T_g, T_m, crystallization temperatures (T_{cc}), and the corresponding specific enthalpy values (ΔH_m, ΔH_{cc}) of the blend constituents were thus obtained. Equation (1) shows how the degree of crystallinity (χ) of the PLA phase in the blends was evaluated.

$$\chi = \frac{\Delta H_m - \Delta H_{cc}}{\Delta H_m^* \cdot w} \cdot 100 \tag{1}$$

where ΔH_{cc} is the enthalpy of cold crystallization of the PLA in the blend, while ΔH_m^* is the enthalpy of melting of fully crystalline PLA, taken equal to 93.7 J/g,[68] while ω is the weight fraction of PLA in the blend.

Thermogravimetric analysis (TGA) was performed through a Mettler TG50IR thermobalance (Mettler Toledo Inc.), testing samples of approximately 5 mg at 10°C/min from 35°C up to 700°C, under nitrogen flow of 100 ml/min. This test allowed the calculation of the initial mass loss (m_{loss}) at a temperature of 185°C, related to residual solvent and absorbed moisture evaporation, of the maximum degradation temperature (T_D), considered as the peak of the mass loss derivative (DTG) curve, and of the residual mass at 700°C (m_{700}).

2.3.3 | Mechanical properties

Regarding the mechanical properties, quasi-static tensile tests were carried out at room temperature by using an Instron® 5969 tensile testing machine equipped with a 100 N load cell. Fibers were fixed on paper frame supports with a gauge length of 50 mm and tested at a crosshead speed of 1 mm/min. At least six specimens were tested for each composition. In this way, the determination of the

elastic modulus (E), of the stress at yield (σ_y), and of the failure properties (σ_b, and ε_b) was performed.

3 | RESULTS AND DISCUSSIONS

3.1 | Microstructural and chemical properties

Figure 2a,b reports the micrographs of the cross-sections of the as-spun fibers obtained through light microscopy. The as-spun fibers were characterized by a non-circular cross-section, which could be explained by possible deformation caused by the contact between the fibers emerging from the non-solvent bath, which have some solvent residues and are thus easily deformable, and the take-up rolls. Nevertheless, further analysis will be needed to better understand the mechanism driving the formation of fibers characterized by this peculiar shape. Interestingly, PLA_20PPeF fibers report a marked crenulated cross-section, different from that of neat PLA ones. The crenulation phenomena arise as soon as the solvent starts to diffuse out in the non-solvent bath, resulting in an increase of the surface area that could lead to better solvent diffusion in the non-solvent bath during the wet spinning process. To quantify the crenulation phenomena, both the perimeter and the area of the cross-section of the fibers have been measured. PLA_20PPeF fibers possess a perimeter to area ratio of 7.2 ± 2.0 mm^{-1}, while PLA fibers have a perimeter to area ratio of 5.5 ± 0.4 mm^{-1}. Therefore, the perimeter to area ratio of PLA_20PPeF fibers is 31% higher than that of PLA ones, meaning that the addition of PPeF to PLA leads to more pronounced crenulation phenomena. As already seen in Table 1, the addition of PPeF to PLA does not substantially change the mean diameter of the fibers. Moreover, as it is possible to notice from Figure 2b, PPeF domains are homogeneously distributed within the PLA matrix and their size in the center (3.7 ± 0.8 µm) is higher than in the boundaries (1.6 ± 0.3 µm). This could be explained considering that PPeF has a higher affinity to chloroform

with respect to PLA and thus, during the spinning process, PPeF domains tend to aggregate in the chloroform-rich region, that is, in the center of the fibers. From the obtained micrographs, it can be noticed that PLA and PPeF phases are completely immiscible in the prepared fibers.

Figure 3a,b reports FESEM micrographs of the lateral surface of neat PLA and PLA_30PPeF fiber blends. As it is possible to notice in Figure 3a, the lateral surface of as-spun PLA is smooth and regular. A similar morphology was highlighted in a work of Gupta et al.,[69] in which PLA fibers were prepared by dry-jet-wet spinning. According to light microscopy analysis, PLA_30PPeF fiber shows a highly crenulated lateral surface, without the presence of pores (Figure 3b).

Figure 4a–f show FESEM micrographs of the cryo-fracture surface of PLA, PLA_30PPeF, and PLA_50PPeF fiber blends at two different magnification levels, that is, 5000x (Figure 4a–c) and 20,000× (Figure 4d–f). A porous internal microstructure can be seen in the cryofracture surface of the PLA fiber (Figure 4a,d), with a mean pore size of 0.8 ± 0.2 µm, and a similar porosity can be detected in the PLA phase of all the produced fiber blends. In a similar work on dry-jet-wet spinning of PLA fibers, the Authors observed that the cross-section of the fibers was characterized by the same porous microstructure.[70] Furthermore, they highlighted that the higher the residence time of the spun fiber in the coagulation bath, the higher was the porosity degree. The suggested explanation of this effect was the complete precipitation of the chloroform in methanol. In the present work, the residence time of the fiber in the non-solvent bath was quite long, approximately six times longer than that adopted by Gupta et al.,[70] and therefore the observed porosity level is expected to be rather high. In the work of Liu et al.,[71] the production of PLA fibers through airflow bubble-spinning was investigated. They observed that the lateral surface of the fibers through SEM exhibited grooved structures. The proposed explanation for such morphology was a combination of low temperature and incomplete solvent evaporation.
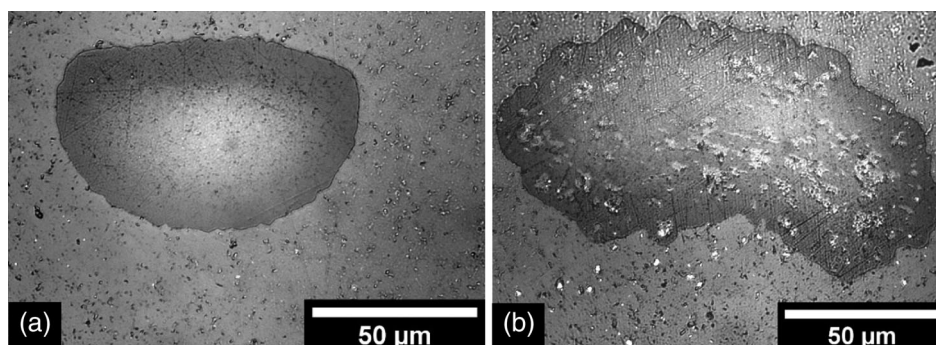

FIGURE 2 Cross-section of the fiber blends obtained through light microscopy: (a) Poly(lactic acid) (PLA) and (b) PLA_20poly (pentamethylene 2,5-furanoate) samples
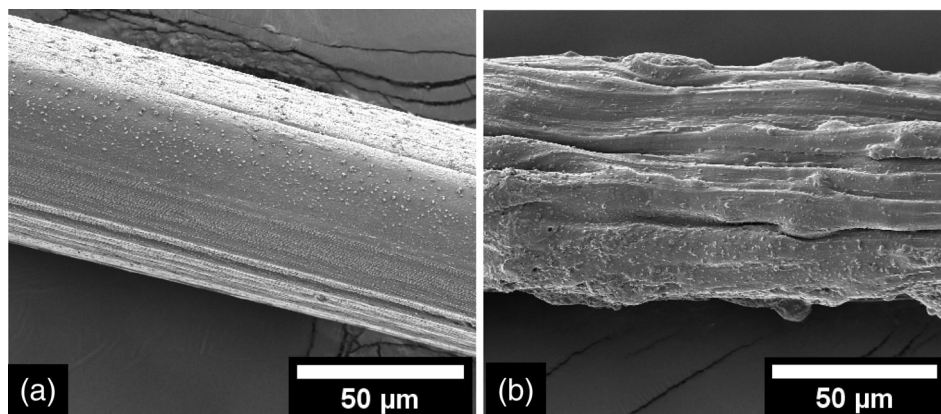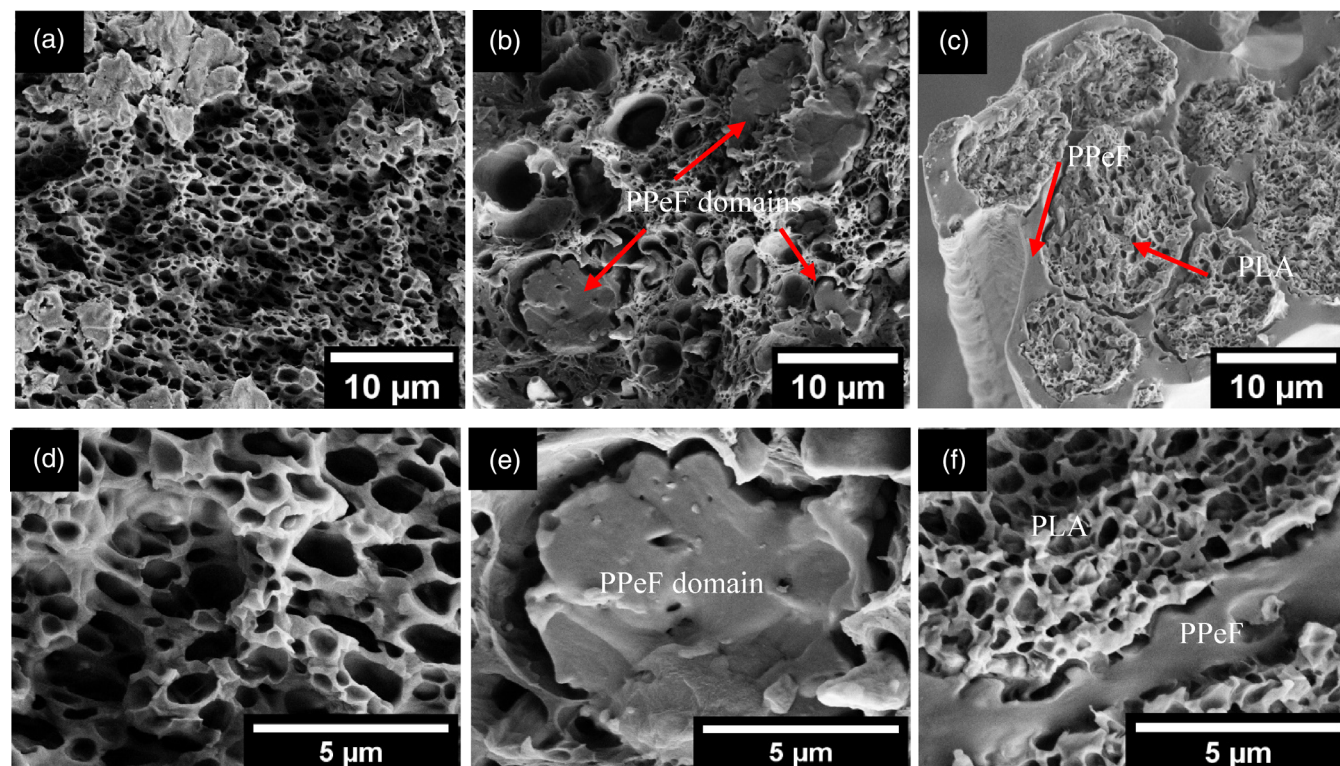
FIGURE 4 Field-emission scanning electron microscopy micrographs of the cryofractured cross-section of the as-spun fibers at a magnification of 5000×: (a) Poly(lactic acid) (PLA), (b) PLA_30poly(pentamethylene 2,5-furanoate) (PPeF), (c) PLA_50PPeF samples, and at a magnification of 20,000×, (d) PLA, (e) PLA_30PPeF, and (f) PLA_50PPeF samples [Color figure can be viewed at wileyonlinelibrary.com]

The cryofracture surface of PLA_30PPeF fiber (Figure 4b) shows that domains of PPeF, having a mean size of 3.7 ± 1.2 μm, are homogeneously distributed in the PLA matrix. If the same sample is observed at higher magnification (Figure 4e), it is possible to see that there is limited interfacial interaction between PLA and PPeF, underlining thus their poor miscibility. The observed lack of interfacial adhesion could lead to a strong decrease in the mechanical properties of the resulting fibers. Figure 4c reports the cryofracture surface of PLA_50PPeF sample. At this PPeF concentration, a phase inversion occurs between PLA and PPeF, with pores in the PLA phase characterized

by a mean diameter of 0.8 ± 0.2 μm. In the micrograph of PLA_50PPeF at higher magnification, (see Figure 4f) the limited compatibility between the two phases is confirmed.

Figure 5a–d shows the ATR-FTIR baseline-corrected spectra of the produced fibers and of the as received PPeF. In the 2800–3000 cm^{-1} region of all the obtained spectra, the characteristic CH_3 asymmetric signal at 2998 cm^{-1} and the CH_3 asymmetric signal at 2940 cm^{-1} can be detected (Figure 5b). The C=O stretching signal is located at 1744 cm^{-1}, and both C—H asymmetric and symmetric bending can be observed at 1448 and 1352 cm^{-1}, respectively (Figure 5c). In addition, the C—O—C stretching
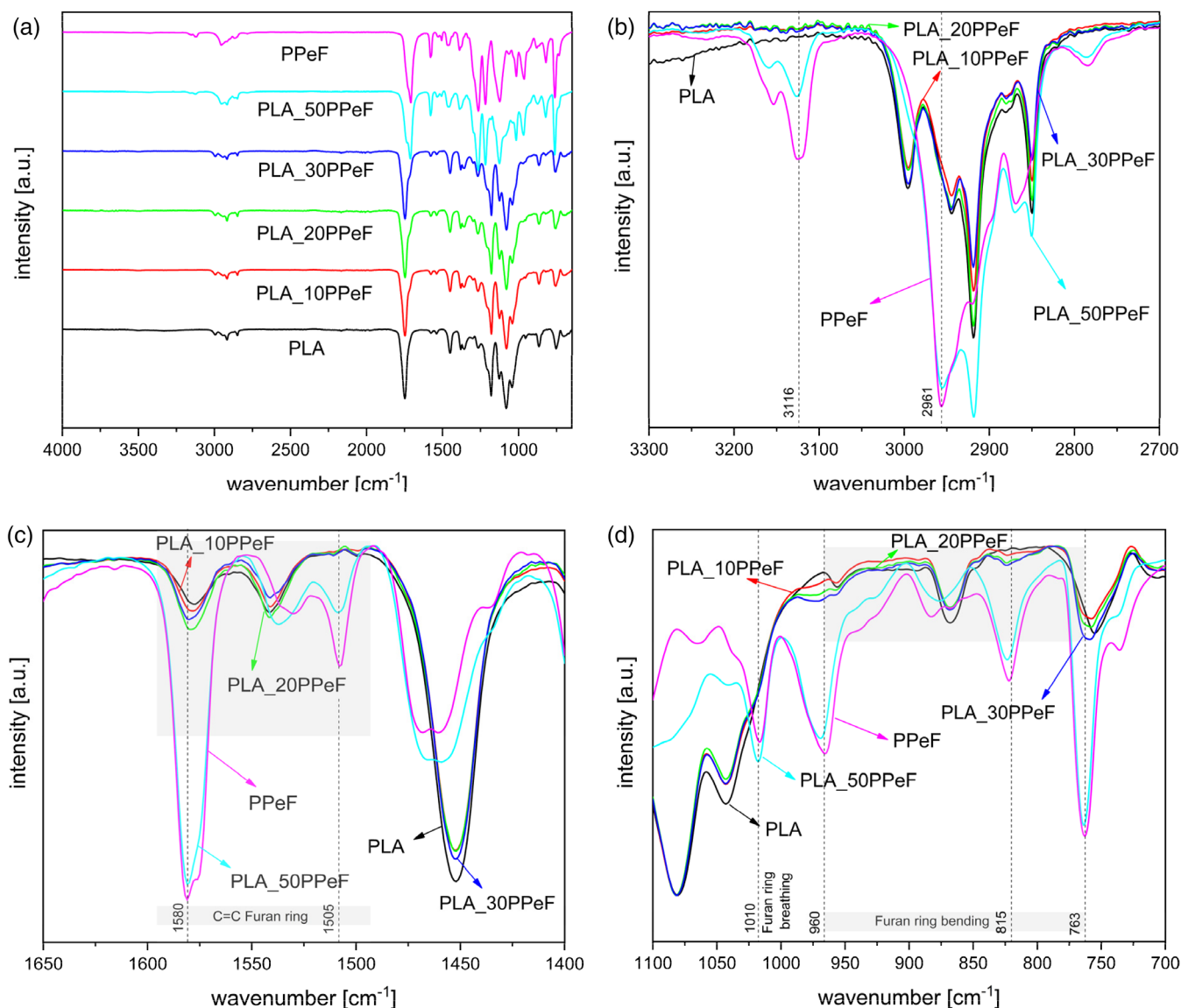
FIGURE 5 (a) Vertically translated attenuated total reflectance-Fourier transformed infrared spectra of the fiber blends and of the poly(pentamethylene 2,5-furanoate) (PPeF). (b,c,d) Detailed sections of the spectra highlighting the most important vibrations of PPeF [Color figure can be viewed at wileyonlinelibrary.com]

signals can be detected in the region comprised between 1180 and 1080 cm^{-1} (Figure 5d).[72,73] Concerning the neat PPeF spectrum, it shows the characteristic signals of furan-based polymers, that is, the stretching vibration of C—H at 3116 cm^{-1}, the stretching vibration of CH$_3$ at 2961 cm^{-1} (Figure 5b), the stretching vibration of C=C at 1580^{-1} (Figure 5c), furan ring breathing at 1012 cm^{-1} and furan ring bending at 962 cm^{-1}, 814 and 763 cm^{-1} (Figure 5d). Furthermore, in the spectra of the as received PPeF the characteristic peaks of ester bonds such as C=O at 1708 cm^{-1} and C—O in the region 1272–1121 cm^{-1} can be clearly detected.[74] In Figure 5d it is possible to notice two different peaks related to the crystalline and the amorphous phase of PLA. The peak corresponding to the

crystalline phase is located at 868 cm^{-1}, while the peak related to the amorphous phase is located at 755 cm^{-1}, as already reported in the literature.[75,76] These results confirmed that the produced fibers are semi-crystalline, as reported in the DSC analysis. Regarding the spectra of the fiber blends, it is interesting to notice that for a concentration of PPeF up to 30 wt% only the characteristic peaks of PLA can be detected, while at higher concentration, i.e., 50 wt% of PPeF, the characteristic peaks of PPeF appear in the spectrum together with those of PLA. The possible explanation for this experimental evidence can be referred to both the microstructure of the fibers and to the penetration depth of the FTIR technique. In fact, ATR-FTIR spectroscopy is a bulk technique, since it has a

penetration depth of 2 μm. Thus, by looking at the microstructure of the fibers (see Figure 2), being the domains of PPeF homogenously distributed in the PLA matrix until a PPeF content of 30 wt%, the outer surface of the fiber is composed only by PLA, and the probability of detecting the signals of PPeF domains is thus rather low. On the other hand, the probability to detect through FTIR the chemical features of the PPeF phase increases consistently in PLA_50PPeF fiber, since phase inversion occurred for this sample (see Figure 4c,e). In conclusion, FTIR spectra of the prepared fibers suggest that all the peaks related to the neat polymer constituents can be easily detected, without any significant intensity variation or red- or blue-shift, and without the formation of new chemical bonds between PLA and PPeF, indicating that there is no chemical interaction between PLA and PPeF phases, and confirming thus the immiscibility of the prepared blends.

3.2 | Thermal properties

Figure 6a,b show the DSC thermograms of the produced fibers and of the as received PPeF sample, while in Table 2 are reported the most important results obtained from these tests. Figure 6a reports the thermograms referring to the first heating scan, and it is possible to notice that the as received PPeF utilized in this work is fully amorphous, showing a T_g at 17.2°C, which is a temperature close to that found in literature for this material.[43] Being amorphous is a characteristic of the polyesters with a C-odd-numbered glycolic subunit, like PPeF, while those with a C-even-numbered glycolic subunit, such as PBF, POF, PDeF, tend to develop a crystalline structure.[44,51,77] Furthermore, PLA exhibits a T_g at 54.1°C,

a cold crystallization peak at 96.5°C, and an endothermic melting peak at 166.2°C. Interestingly, both the T_g and the T_m of PLA are unaltered by the addition of PPeF, and this further confirms that PLA and PPeF are immiscible. During the first heating scan (Figure 6a), a small cold crystallization peak referring to the PLA phase can be detected, and the crystalline content in the PLA fibers is approximately 27.2%. Regarding the crystalline content of PLA in the produced blends, it seems to increase by increasing the PPeF concentration up to 20 wt%, while it decreases for higher PPeF amounts. In addition, the T_{cc} related to the PLA phase seems to decrease with the PPeF content. Thus, the crystallinity of PLA is considerable after wet spinning, but, after the first DSC cycle, the thermal history of the material is erased, which results in a nearly fully amorphous PLA undergoing cold crystallization upon second heating. Furthermore, the presence of PPeF domains inside the PLA matrix seems to favor the cold crystallization of PLA, as they could act as a nucleating agent, increasing the crystalline content from 27.2% to 40.7% for the composition containing 20 wt% of PPeF. A slightly lower increase in the crystallinity in the PLA phase was observed in the work of Quero et al. on PLA/PBAT blends.[78] Furthermore, a similar enhancement in the crystallinity content in PLA phase was also reported by Shikui et al.[79] They investigated the effect of the addition of graphene oxide (GO) and polyethylene glycol (PEG) to PLA and they highlighted that both GO and PEG act as nucleating agents, decreasing T_{cc} and increasing the crystalline content from 5.5% to 39.3%. Interestingly, the melting behavior of PLA is characterized by the appearance of double melting peaks that could be caused by two different phenomena. The first phenomenon is correlated to the crystallization process
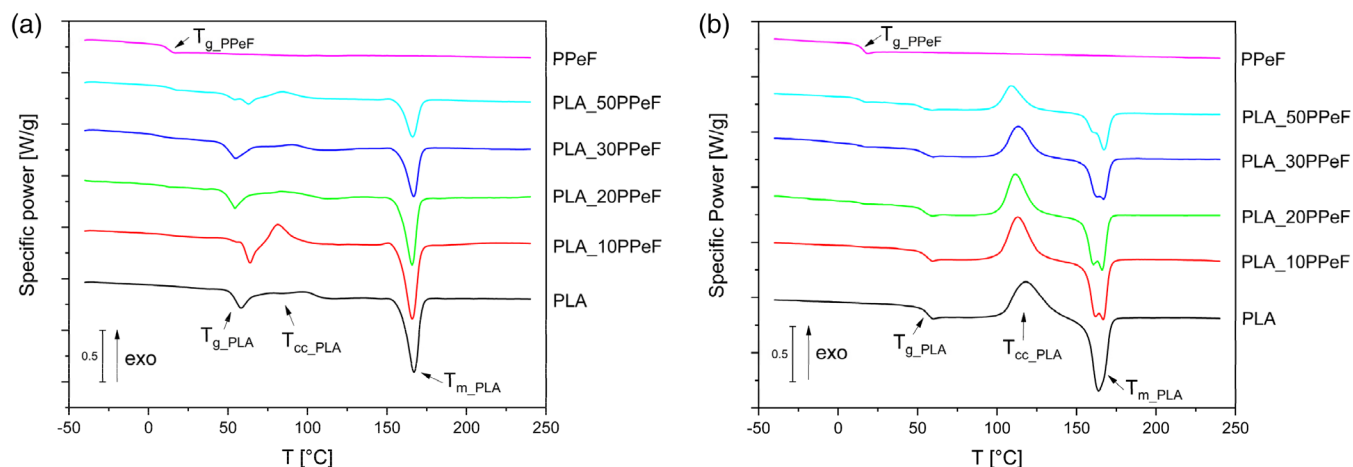

FIGURE 6 Differential scanning calorimetry thermograms of poly(pentamethylene 2,5-furanoate) (PPeF), neat poly(lactic acid) (PLA), and PLA_xPPeF fiber blends (x = 10–50 wt%). (a) First heating scan, (b) second heating scan [Color figure can be viewed at wileyonlinelibrary.com]

TABLE 2 Results of differential scanning calorimetry tests on poly(pentamethylene 2,5-furanoate) (PPeF), neat poly(lactic acid) (PLA) and PLA_xPPeF fiber blends ($x = 10$–50 wt%)

First heating scan							
Sample	$T_{g\ PPeF}$ (°C)	$T_{g\ PLA}$ (°C)	T_{cc} PLA (°C)	ΔH_{cc} PLA (J/g)	T_m PLA (°C)	$\Delta H_{m\ PLA}$ (J/g)	χ PLA (%)
PLA	–	54.1	96.5	12.0	166.2	37.6	27.2
PLA_10PPeF	10.8	60.8	81.2	15.4	164.9	38.1	26.9
PLA_20PPeF	10.9	51.5	83.4	1.0	165.4	31.5	40.7
PLA_30PPeF	8.1	51.0	90.2	0.9	166.2	24.0	35.2
PLA_50PPeF	13.9	50.2	84.8	5.2	165.5	19.6	30.7
PPeF	17.2	–	–	–	–	–	–
Second heating scan							
PLA	–	56.1	118.1	39.9	163.1	44.0	4.4
PLA_10PPeF	14.7	54.7	113.0	40.6	166.0	37.4	3.2
PLA_20PPeF	12.1	55.2	101.7	33.9	165.8	36.3	3.2
PLA_30PPeF	14.6	53.1	102.7	26.7	166.6	27.0	0.5
PLA_50PPeF	13.4	51.6	98.9	20.3	158.7	20.9	1.3
PPeF	17.2	–	–	–	–	–	–

Abbreviations: χ_{PLA}, crystallinity content of PLA; ΔH_{cc_PLA}, crystallization enthalpy of PLA; ΔH_{m_PLA}, melting enthalpy of PLA; T_{cc_PLA}, crystallization temperature of PLA; T_{g_PLA}, glass transition temperature of PLA; T_{g_PPeF}, glass transition temperature of PPeF; T_{m_PLA}, melting temperature of PLA.
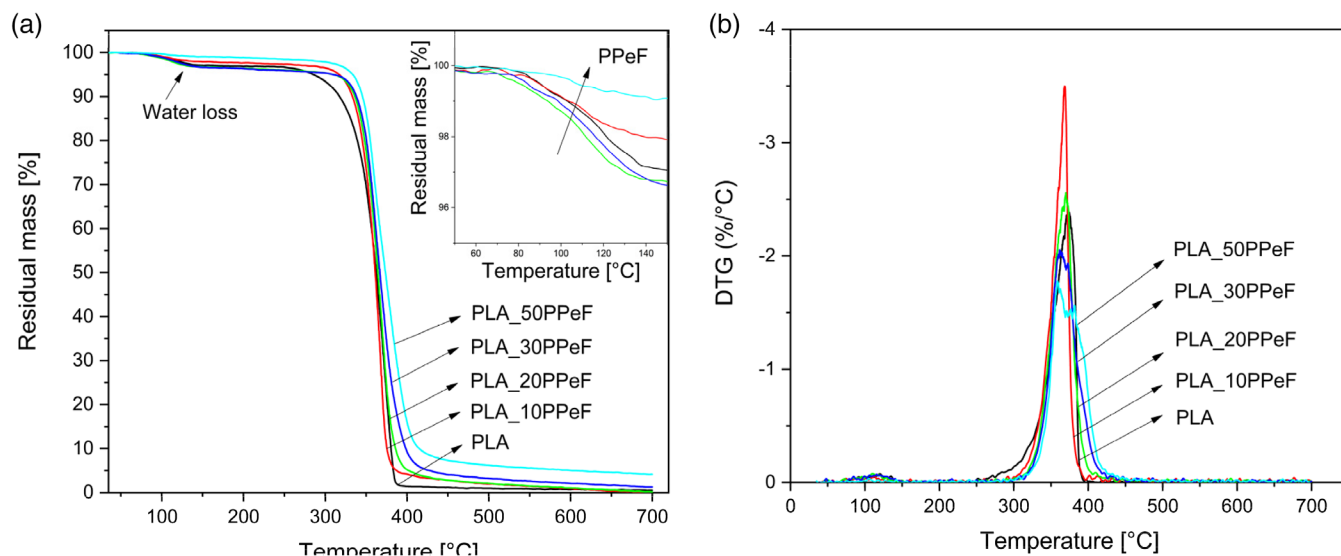

FIGURE 7 Thermogravimetric analysis thermograms of neat poly(lactic acid) (PLA) and PLA_xpoly(pentamethylene 2,5-furanoate) fiber blends ($x = 10$–50 wt%). (a) Residual mass and (b) mass loss derivative [Color figure can be viewed at wileyonlinelibrary.com]

occurring during the cooling scan, which corresponds to the partial recrystallization of PLA mesophase into more stable α-crystals, and thus resulting in a double melting peak since the two crystalline phases are characterized by different thermal stability.[80] As reported in the work of Quero et al.,[78] the double endothermic peaks related to the melting of PLA phase tend to disappear as the heating rate increases. Similar results were observed also

by Yasuniwa et al.[81] The second phenomenon can be related to the melting of PLA crystals characterized by different lamellae thickness and therefore possessing different thermal stability.[82]

Figure 7a,b reports TGA thermograms and DTG curves of PLA/PPeF fiber blends, while the main results in terms of mass loss, degradation temperature, and residual mass at 700°C are reported in Table 3. In the thermograms of

TABLE 3 Results of the thermogravimetric analysis tests of poly(lactic acid) (PLA) and PLA_xpoly(pentamethylene 2,5-furanoate) fiber blends (x = 10–50 wt%)

Sample	m_{loss} [%]	T_D (°C)	m_{700} (%)
PLA	3.1	373.7	0.49
PLA_10PPeF	2.3	368.2	0.10
PLA_20PPeF	3.5	369.8	0.16
PLA_30PPeF	3.5	361.5	1.24
PLA_50PPeF	1.0	358.7	4.13

Abbreviations: m_{loss}, mass loss; m_{700}, residual mass at 700°C; T_D, maximum degradation temperature.

the fiber blends (Figure 7a) a mass loss starting at around 80°C can be detected, and it can be probably related both to the evaporation of the absorbed water within the material and to the presence of residual traces of solvent. In addition, by increasing the content of PPeF to 50 wt%, the initial mass loss significantly decreases. PPeF is characterized by excellent barrier properties and therefore, its addition leads to a decrease in the hygroscopicity of PLA. Furthermore, the thermal degradation at elevated temperature of PLA is not dramatically affected by the presence of PPeF in the blends (see T_D values in Table 3). The slight drop of T_D upon PPeF addition should not limit the maximum service temperature of these blends. Similar results regarding the T_D were obtained in the work of Ozdemir et al.[83] concerning the preparation of PLA/poly(ethylene glycol) fibers. Furthermore, by looking at the thermograms reported in Figure 7a, at a temperature of 400°C the degradation of PLA is almost complete, while the degradation process of PPeF is not yet concluded. Figure 7b reports the DTG curves of all the produced fiber blends in which it can be noticed that PLA reports a T_D approximately at 370°C, while the PPeF is characterized by a slightly lower maximum decomposition temperature, that is, 350°C.[44] Furthermore, the m_{700} values tend to increase by increasing the PPeF content in the blends, meaning that PPeF degradation leads to the production of non-volatile products.

3.3 | Mechanical properties

Figure 8 shows representative stress–strain curves from quasi-static tensile tests on neat PLA and PLA_xPPeF fiber blends (x = 10–50 wt%), while the main results are collected in Table 4. PLA fibers show an elevated elastic modulus, approx. 2.2 GPa, and good failure properties, with a stress at break of 30.1 MPa and a strain at break of 127%. The obtained values are in good agreement with the data reported in the literature on melt spun PLA
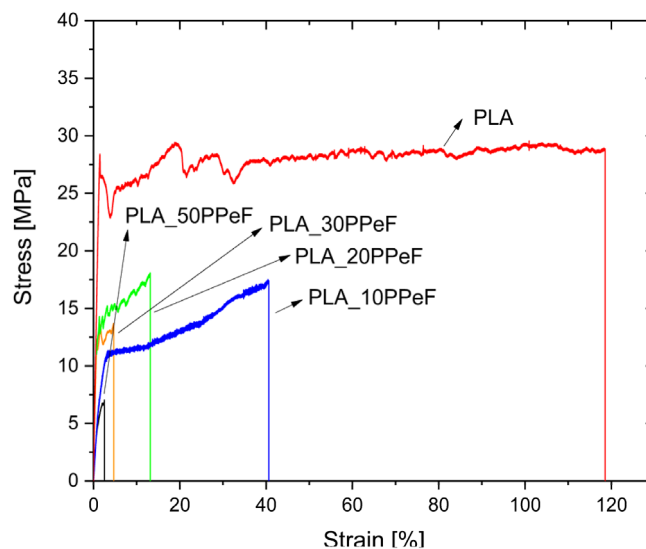

FIGURE 8 Stress–strain curves from quasi-static tensile tests on neat poly(lactic acid) (PLA) and PLA_xpoly(pentamethylene 2,5-furanoate) fiber blends (x = 10–50 wt%) [Color figure can be viewed at wileyonlinelibrary.com]

fibers.[84] Regarding the mechanical properties of the produced PLA_xPPeF fiber blends, it is possible to notice that they tend to progressively decrease by increasing the PPeF concentration. A drop in the elastic modulus values was expected, considering the intrinsic low stiffness of PPeF used in this work. The stiffness of the furanoates decreases with the number of carbon atoms in the alkyl chain, but their elongability improves[36,41–44]. As reported by Guidotti et al.[44], PPeF is characterized by a limited yield resistance thus leading to an overall decrease in the yield stress of the produced blends by increasing its content. Furthermore, the observed decrease in the yield stress could be correlated to the rather poor interfacial adhesion between PLA and PPeF phases, as reported in FESEM micrographs (see Figure 4).[85] For the same reason, both the stress and the strain at break significantly decrease with the PPeF amount. At a PPeF concentration of 50 wt%, the ε_b decreases up to 1.9%, and also σ_b drops down to 3.5 MPa. For this sample, the observed drop in the mechanical properties could be also attributed to the phase inversion observed in the FESEM micrographs reported in Figure 4c,f. A decrease in the mechanical properties due to the phase separation of the blend constituents was also reported by Jompang et al.[86] In their work, PLA/poly(butylene succinate) (PBS) fibers were obtained through melt spinning, and the observed decrease in the mechanical properties with the PBS addition was correlated to the phase separation occurring in the fibers. It can be therefore concluded that the poor adhesion between PLA and PPeF does not allow exploiting the elevated ductility of the PPeF phase within the

TABLE 4 Results of quasi-static tensile tests on neat poly(lactic acid) (PLA) and PLA_$x$poly(pentamethylene 2,5-furanoate) (PPeF) fiber blends ($x = 10$–50 wt%)

Sample	E (GPa)	σ_y (MPa)	σ_b (MPa)	ε_b (%)
PLA	2.2 ± 0.4	30.6 ± 3.9	30.1 ± 4.1	127.0 ± 48.0
PLA_10PPeF	0.9 ± 0.3	10.8 ± 2.9	14.3 ± 2.1	54.0 ± 12.0
PLA_20PPeF	1.7 ± 0.6	9.3 ± 3.3	13.3 ± 4.8	10.3 ± 5.4
PLA_30PPeF	1.5 ± 0.8	9.6 ± 3.0	13.1 ± 4.5	2.9 ± 1.4
PLA_50PPeF	0.6 ± 0.2	-	3.5 ± 1.8	1.9 ± 1.8

Abbreviations: E, elastic modulus; ε_b, strain at break; σ_b, stress at break; σ_y, yield stress.

prepared blends. It can be hypothesized that at elevated strain levels PPeF domains are completely debonded from the PLA matrix, hindering thus the load transfer and the deformation of the PPeF phase.

In order to improve the mechanical properties of these fiber blends, it should be necessary to introduce some compatibilizers, able to produce a better dispersion of PPeF domains within PLA, reducing also their size and increasing the interfacial adhesion. The most widely used compatibilizers for PLA are maleic anhydride (MAH) and isocyanates derivatives groups. Polymers grafted with MAH, like PP-g-MAH[87] and PLA-g-MAH,[88] have been extensively used for improving the compatibility among the PLA and TPS constituents of the blends, respectively. Moreover, isocyanates derivatives groups enable the formation of urethane groups between isocyanate and the hydroxyl group present in both PLA and TPS.[89] Another possible mechanism to improve the adhesion between PLA and PPeF could be the use of block copolymers of PLA/PPeF. On the other hand, the mechanical properties of these fibers could be also improved by performing a hot drawing at a temperature above the T_g of PLA. This process may induce morphological changes in drawn fibers, like the deformation of the PPeF domains along the strain direction, improving thus the load distribution mechanism and thus the failure properties.

4 | CONCLUSIONS

Wet spinning process has been successfully employed to produce, for the first time, biobased fibers made of PLA and a furan-based polymer, that is, PPeF. A comprehensive characterization of the microstructural, thermal, and mechanical properties of the produced fibers has been carried out. From the micrographs obtained through light microscopy, it was possible to observe the overall cross-section of the produced PLA/PPeF fiber blends, and also the immiscibility of the produced blends was further confirmed by the fact that the PPeF domains homogeneously dispersed within the PLA matrix. Through FESEM both the lateral surface and the cryofracture surface of the

produced fiber blends were analyzed and it was possible to observe that the PLA matrix was porous and also there was a lack of adhesion between PLA matrix and PPeF domains. Furthermore, by increasing the PPeF concentration up to 50 wt% an evident phase inversion occurred. ATR-FTIR spectra highlighted the main absorption peaks related to each polymer phase, without evidencing any chemical interaction between them. DSC tests highlighted that PPeF acted as a nucleating agent enhancing the crystallization kinetics of PLA in the as produced wet-spun fibers, and also in the solid state during cold crystallization. Thus, it is an interesting phenomenon that can positively affect the mechanical properties of the produced fibers and should be considered in the process scale up. Concerning the thermal stability of PLA, it was substantially unaltered by the presence of PPeF, as shown by the TGA analysis. Interestingly, the presence of PPeF in these blends decreased the water absorption propensity of PLA, especially at a PPeF content of 50 wt%. Quasi-static tensile tests reported a remarkable decrease in the mechanical properties of the fiber blends with the PPeF content, probably related to the immiscibility between the blend constituents.

This work highlighted for the first time the possibility to produce through wet spinning bio-derived fiber blends, possessing peculiar microstructural and thermal properties. Further efforts will be made to improve the mechanical performances of these blends, for instance by adding suitable compatibilizers or by inducing a more efficient load transfer mechanism through a hot drawing process.

AUTHORS CONTRIBUTION

All authors contributed to the study conception and design. Material preparation, data collection and analysis were performed by Davide Perin. The first draft of the manuscript was written by Davide Perin and all authors commented on previous versions of the manuscript. All authors read and approved the final manuscript.

CONFLICT OF INTEREST

The authors declare that they have no known competing financial interests or personal relationships that could have appeared to influence the work reported in this paper.

DATA AVAILABILITY STATEMENT

Data and materials are available under requests.

ORCID

Davide Perin https://orcid.org/0000-0002-6248-2012

REFERENCES

[1] L. Lebreton, A. Andrady, *Palgrave Commun.* **2019**, *5*, 6.

[2] A. K. Panda, R. K. Singh, D. K. Mishra, *Renew. Sust. Energ. Rev.* **2010**, *14*, 233.

[3] B. Bai, H. Jin, C. Fan, C. Cao, W. Wei, W. Cao, *Waste Manag.* **2019**, *89*, 247.

[4] B. C. Gibb, *Nat. Chem.* **2019**, *11*, 394.

[5] S. B. Borrelle, C. M. Rochman, M. Liboiron, A. L. Bond, A. Lusher, H. Bradshaw, J. F. Provencher, *Proc. Natl. Acad. Sci.* **2017**, *114*, 9994.

[6] J. Payne, P. McKeown, M. D. Jones, *Polym. Degrad. Stab.* **2019**, *165*, 170.

[7] M. Gross, *Curr. Biol.* **2017**, *27*, R785.

[8] N. Peelman, P. Ragaert, B. De Meulenaer, D. Adons, R. Peeters, L. Cardon, F. Van Impe, F. Devlieghere, *Trends Food Sci. Technol.* **2013**, *32*, 128.

[9] J. B. Van Beilen, Y. Poirier, *Plant J.* **2008**, *54*, 684.

[10] G.-Q. Chen, M. K. Patel, *Chem. Rev.* **2012**, *112*, 2082.

[11] S. Walker, R. Rothman, *J. Clean. Prod.* **2020**, *261*, 121158.

[12] M. Asgher, S. A. Qamar, M. Bilal, H. M. N. Iqbal, *Food Res. Int.* **2020**, *137*, 109625.

[13] E. A. MacGregor, in *Encyclopedia of Physical Science and Technology*, 3d ed. (Ed: R. A. Meyers), Academic Press, New York **2003**.

[14] D. Garlotta, *J. Polym. Environ.* **2001**, *9*, 63.

[15] Z. A. Raza, S. Abid, I. M. Banat, *Int. Biodeterior. Biodegradation* **2018**, *126*, 45.

[16] M. Labet, W. Thielemans, *Chem. Soc. Rev.* **2009**, *38*, 3484.

[17] A. Dorigato, D. Perin, A. Pegoretti, *J. Polym. Environ.* **2020**, *28*, 3244.

[18] M. Aslam, M. A. Kalyar, Z. A. Raza, *Polym. Eng. Sci.* **2018**, *58*, 2119.

[19] M. Tait, A. Pegoretti, A. Dorigato, K. Kalaitzidou, *Carbon* **2011**, *49*, 4280.

[20] A. Dorigato, M. Sebastiani, A. Pegoretti, L. Fambri, *J. Polym. Environ.* **2012**, *20*, 713.

[21] L. Fambri, A. Dorigato, A. Pegoretti, *Appl. Sci.* **2020**, *10*, 6731.

[22] V. P. Martino, A. Jiménez, R. A. Ruseckaite, L. Avérous, *Polym. Adv. Technol.* **2011**, *22*, 2206.

[23] A. Hassan, H. Balakrishnan, A. Akbari, in *Advances in Natural Polymers: Composites and Nanocomposites* (Eds: S. Thomas, P. M. Visakh, A. P. Mathew), Springer, Heidelberg **2013**.

[24] D. R. Paul, in *Polymer Blends* (Eds: D. R. Paul, S. Newman), Academic Press, New York **1978**.

[25] D. A. Brant, *J. Chem. Educ.* **1981**, *58*, A154.

[26] L. H. Sperling, *J. Polym. Sci. Part C Polym. Lett.* **1990**, *28*, 387.

[27] G. H. Fredrickson, A. J. Liu, F. S. Bates, *Macromolecules* **1994**, *27*, 2503.

[28] Y. Qin, in *Medical Textile Materials* (Ed: Y. Qin), Woodhead Publishing, Cambridge **2016**.

[29] A. F. Sousa, C. Vilela, A. C. Fonseca, M. Matos, C. S. R. Freire, G.-J. M. Gruter, J. F. J. Coelho, A. J. D. Silvestre, *Polym. Chem.* **2015**, *6*, 5961.

[30] G. Z. Papageorgiou, D. G. Papageorgiou, Z. Terzopoulou, D. N. Bikiaris, *Eur. Polym. J.* **2016**, *83*, 202.

[31] Z. Terzopoulou, L. Papadopoulos, A. Zamboulis, D. G. Papageorgiou, G. Z. Papageorgiou, D. N. Bikiaris, *Polymers* **2020**, *12*, 1209.

[32] X. Fei, J. Wang, J. Zhu, X. Wang, X. Liu, *ACS Sustainable Chem. Eng.* **2020**, *8*, 8471.

[33] G. Guidotti, L. Genovese, M. Soccio, M. Gigli, A. Munari, V. Siracusa, N. Lotti, *Int. J. Mol. Sci.* **2019**, *20*, 2187.

[34] G. Guidotti, M. Gigli, M. Soccio, N. Lotti, M. Gazzano, V. Siracusa, A. Munari, *Polymers* **2018**, *10*, 167.

[35] G. Guidotti, M. Soccio, N. Lotti, V. Siracusa, M. Gazzano, A. Munari, *Polym. Degrad. Stab.* **2019**, *169*, 108963.

[36] A. Gandini, A. J. D. Silvestre, C. P. Neto, A. F. Sousa, M. Gomes, *J. Polym. Sci.* **2009**, *47*, 295.

[37] A. J. J. E. Eerhart, A. P. C. Faaij, M. K. Patel, *Energy Environ. Sci.* **2012**, *5*, 6407.

[38] M. Vannini, P. Marchese, A. Celli, C. Lorenzetti, *Green Chem.* **2015**, *17*, 4162.

[39] G. Z. Papageorgiou, V. Tsanaktsis, D. G. Papageorgiou, S. Exarhopoulos, M. Papageorgiou, D. N. Bikiaris, *Polymer* **2014**, *55*, 3846.

[40] G. Guidotti, M. Soccio, N. Lotti, M. Gazzano, V. Siracusa, A. Munari, *Polymers* **2018**, *10*, 785.

[41] V. Tsanaktsis, Z. Terzopoulou, M. Nerantzaki, G. Z. Papageorgiou, D. N. Bikiaris, *Mater. Lett.* **2016**, *178*, 64.

[42] G. Guidotti, M. Soccio, M. C. García-Gutiérrez, T. Ezquerra, V. Siracusa, E. Gutiérrez-Fernández, A. Munari, N. Lotti, *ACS Sustainable Chem. Eng.* **2020**, *8*, 9558.

[43] D. E. Martínez-Tong, M. Soccio, B. Robles-Hernández, G. Guidotti, M. Gazzano, N. Lotti, A. Alegria, *Macromolecules* **2020**, *53*, 10526.

[44] G. Guidotti, M. Soccio, M.-C. García-Gutiérrez, E. Gutiérrez-Fernández, T. A. Ezquerra, V. Siracusa, A. Munari, N. Lotti, *ACS Sustain. Chem. Eng.* **2019**, *7*, 17863.

[45] J. Ma, Y. Pang, M. Wang, J. Xu, H. Ma, X. Nie, *J. Mater. Chem.* **2012**, *22*, 3457.

[46] G. Papageorgiou, N. Guigo, V. Tsanaktsis, D. Papageorgiou, S. Exarhopoulos, N. Sbirrazzuoli, D. Bikiaris, *Eur. Polym. J.* **2015**, *68*, 115.

[47] V. Tsanaktsis, D. N. Bikiaris, N. Guigo, S. Exarhopoulos, D. G. Papageorgiou, N. Sbirrazzuoli, G. Z. Papageorgiou, *RSC Adv.* **2015**, *5*, 74592.

[48] G. Fredi, A. Dorigato, M. Bortolotti, A. Pegoretti, D. Bikiaris, *Polymers* **2020**, *12*, 2459.

[49] D. G. Papageorgiou, N. Guigo, V. Tsanaktsis, S. Exarhopoulos, D. N. Bikiaris, N. Sbirrazzuoli, G. Z. Papageorgiou, *Ind. Eng. Chem. Res.* **2016**, *55*, 5315.

[50] M. Gomes, A. Gandini, A. J. D. Silvestre, B. Reis, *J. Polym. Sci. A Polym. Chem.* **2011**, *49*, 3759.

[51] G. Papamokos, T. Dimitriadis, D. N. Bikiaris, G. Z. Papageorgiou, G. Floudas, *Macromolecules* **2019**, *52*, 6533.

[52] N. Poulopoulou, G. Kantoutsis, D. N. Bikiaris, D. S. Achilias, M. Kapnisti, G. Z. Papageorgiou, *Polymers (Basel)* **2019**, *11*, 937.

[53] Y. Long, R. Zhang, J. Huang, J. Wang, J. Zhang, N. Rayand, G.-H. Hu, J. Yang, J. Zhu, *Polymer* **2017**, *125*, 138.

[54] Y. Long, R. Y. Zhang, J. C. Huang, J. G. Wang, Y. H. Jiang, G. H. Hu, J. Yang, J. Zhu, *ACS Sustainable Chem. Eng.* **2017**, *5*, 9244.

[55] G. Fredi, D. Rigotti, D. N. Bikiaris, A. Dorigato, *Polymer* **2021**, *218*, 123527.

[56] O. Avinc, A. Khoddami, *Fibre Chem.* **2009**, *41*, 391.

[57] M. Mutsuga, Y. Kawamura, K. Tanamoto, *Food Addit. Contaminants: Part A* **2008**, *25*, 1283.

[58] S. Pivsa-Art, N. Srisawat, N. O-Charoen, S. Pavasupree, W. Pivsa-Art, *Energy Procedia* **2011**, *9*, 589.

[59] K. E. Perepelkin, *Fibre Chem.* **2002**, *34*, 85.

[60] W. Hoogsteen, A. R. Postema, A. J. Pennings, G. Ten Brinke, P. Zugenmaier, *Macromolecules* **1990**, *23*, 634.

[61] J. Lunt, A. L. Shafer, *J. Ind. Text.* **2000**, *29*, 191.

[62] N. Poulopoulou, N. Kasmi, M. Siampani, Z. N. Terzopoulou, D. N. Bikiaris, D. S. Achilias, D. G. Papageorgiou, G. Z. Papageorgiou, *Polymers* **2019**, *11*, 556.

[63] A. Codou, N. Guigo, J. G. van Berkel, E. de Jong, N. Sbirrazzuoli, *J. Polym. Eng.* **2017**, *37*, 869.

[64] S. Sato, D. Gondo, T. Wada, S. Kanehashi, K. Nagai, *J. Appl. Polym. Sci.* **2013**, *129*, 1607.

[65] M. Sajid, X. Zhao, D. Liu, *Green Chem.* **2018**, *20*, 5427.

[66] S. Bello, P. Méndez-Trelles, E. Rodil, G. Feijoo, M. T. Moreira, *Sep. Purif. Technol.* **2020**, *233*, 116056.

[67] G. Fredi, H. Bruenig, R. Vogel, C. Scheffler, *Express Polym. Lett.* **2019**, *13*, 1071.

[68] S. M. Davachi, B. Kaffashi, *Int. J. Polym. Mater. Polym. Biomater.* **2015**, *64*, 497.

[69] B. Gupta, N. Revagade, N. Anjum, B. Atthoff, J. Hilborn, *J. Appl. Polym. Sci.* **2006**, *100*, 1239.

[70] B. Gupta, N. Revagade, N. Anjum, B. Atthoff, J. Hilborn, *J. Appl. Polym. Sci.* **2006**, *101*, 3774.

[71] F. Liu, S. Li, Y. Fang, F. Zheng, J. Li, J. He, *Appl. Surf. Sci.* **2017**, *421*, 61.

[72] B. W. Chieng, N. A. Ibrahim, W. M. Z. W. Yunus, M. Z. Hussein, *Polymers* **2014**, *6*, 93.

[73] N.,. T. Paragkumar, D. Edith, J.-L. Six, *Appl. Surf. Sci.* **2006**, *253*, 2758.

[74] H. Xie, L. Wu, B.-G. Li, P. Dubois, *Polymer* **2018**, *155*, 89.

[75] C. Migliaresi, D. Cohn, A. De Lollis, L. Fambri, *J. Appl. Polym. Sci.* **1991**, *43*, 83.

[76] G. Kister, G. Cassanas, M. Vert, *Polymer* **1998**, *39*, 267.

[77] M. Soccio, D. E. Martínez-Tong, A. Alegría, A. Munari, N. Lotti, *Polymer* **2017**, *128*, 24.

[78] E. Quero, A. J. Müller, F. Signori, M.-B. Coltelli, S. Bronco, *Macromol. Chem. Phys.* **2012**, *213*, 36.

[79] S. Jia, D. Yu, Y. Zhu, Z. Wang, L. Chen, L. Fu, *Polymers* **2017**, *9*, 528.

[80] M. L. Di Lorenzo, R. Androsch, *Polym. Int.* **2019**, *68*, 320.

[81] M. Yasuniwa, S. Tsubakihara, Y. Sugimoto, C. Nakafuku, *J. Polym. Sci. Part B-Polym. Phys.* **2004**, *42*, 25.

[82] C. A. Gracia-Fernández, S. Gómez-Barreiro, J. López-Beceiro, S. Naya, R. Artiaga, *J. Mater. Res.* **2012**, *27*, 1379.

[83] E. Ozdemir, J. Hacaloglu, *J. Anal. Appl. Pyrolysis* **2018**, *129*, 181.

[84] R. L. Shogren, G. Selling, J. L. Willett, *J. Polym. Environ.* **2011**, *19*, 329.

[85] A. Dorigato, A. Pegoretti, A. Frache, *J. Therm. Anal. Calorim* **2012**, *109*, 863.

[86] L. Jompang, S. Thumsorn, J. W. On, P. Surin, C. Apawet, T. Chaichalermwong, N. Kaabbuathong, N. O-Charoen, N. Srisawat, *Energy Procedia* **2013**, *34*, 493.

[87] S. Pivsa Art, J. Kord-Sa Ard, W. Pivsa Art, R. Wongpajan, N. O-Charoen, S. Pavasupree, H. Hamada, *Energy Procedia* **2016**, *89*, 353.

[88] M. A. Huneault, H. Li, *Polymer* **2007**, *48*, 270.

[89] S. Karagoz, G. Ozkoc, *Polym. Eng. Sci.* **2013**, *53*, 2183.